THE JOURNAL OF PHYSICAL CHEMISTRY C
A JOURNAL OF THE AMERICAN CHEMICAL SOCIETY

pubs.acs.org/JPCC
Article

Femtosecond Electron-Transfer Dynamics across the D_2O/Cs^+/Cu(111) Interface: The Impact of Hydrogen Bonding

John Thomas, Jayita Patwari, Inga Christina Langguth, Christopher Penschke, Ping Zhou, Karina Morgenstern, and Uwe Bovensiepen*

Cite This: J. Phys. Chem. C 2023, 127, 23467−23474
Read Online
ACCESS | Metrics & More | Article Recommendations

ABSTRACT: Hydrogen bonding is essential in electron-transfer processes at water−electrode interfaces. We study the impact of the H-bonding of water as a solvent molecule on real-time electron-transfer dynamics across a Cs^+−Cu(111) ion−metal interface using femtosecond time-resolved two-photon photoelectron spectroscopy. We distinguish in the formed water−alkali aggregates two regimes below and above two water molecules per ion. Upon crossing the boundary of these regimes, the lifetime of the excess electron localized transiently at the Cs^+ ion increases from 40 to 60 fs, which indicates a reduced alkali−metal interaction. Furthermore, the energy transferred to a dynamic structural rearrangement due to hydration is reduced from 0.3 to 0.2 eV concomitantly. These effects are a consequence of H-bonding in the water−water interaction and the beginning formation of a nanoscale water network. This finding is supported by real-space imaging of the solvatomers and vibrational frequency shifts of the OH stretching and bending modes calculated for these specific interfaces.

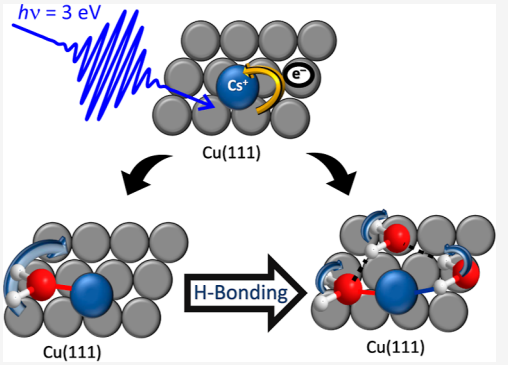

1. INTRODUCTION

Ion−solvent interactions at the nanoscale and electron transfer across heterogeneous interfaces are the key factors for energy storage and energy conversion applications.[1,2] Since the past decade, a number of experimental and theoretical[3−5] investigations have been performed to understand the structural and dynamic properties of such interfaces. Among the widely investigated solvents, water has received special attention because of its wide abundance and relevance of hydration dynamics in various fields like ion transport through membrane channels and nanoconfined environments[6−8] to ion diffusion in energy conversion systems.[9,10] In living cells, water is considered to be a versatile and adaptive component because it combines the properties of a small molecule solvent with hydrogen bonding.[11] Alkali−water interactions at metal interfaces involve a complex interplay of several mechanisms such as hydrogen bonding, van der Waals interaction, and image charge effects.[12] Among the interactions relevant for the polar protic solvent water, H-bonding is fundamental since it influences the electronic and geometric structure and, consequently, the hydration dynamics of the complex multi-component system.[13]

Hydrogen bonding is key in the hydration process and ubiquitous in nature.[13,14] Being stronger than most other intermolecular interactions, hydrogen bonds can be decisive for the structural and dynamical properties of nanoscale systems. It allows, for example, to facilitate tuning biological electron-transfer rates.[15] Recently, this concept has been extended to photocatalytic reactions[16] and electrochemical interfaces[17] where H-bonding has been tuned to regulate the electron-transfer efficiency to benefit the particular application. Thus, at interfaces, the influence of H-bonding on electron transfer is scientifically and technologically important.

Vibrational spectroscopy along with different theoretical models provided significant insights into the influence of hydrogen bonding on solvent networks. Upon H-bonding, the O−H stretch vibration frequency red-shifts by about 10%, and the bending modes exhibit a weaker blue-shift.[13] H-bonding among water influences each of the possible motion of water molecules in a solvent network such as stretching, in-plane bending, and libration.[18] However, real-time information about the dynamics is challenging to obtain experimentally.[19] Time-resolved spectroscopy facilitated probing different dynamical processes on femto- to picoseconds which are relevant in H-bonding.[20] Since such studies were performed in the bulk, the contribution arising from individual water molecules could not be derived due to the large number of water molecules. At

Received: September 13, 2023
Revised: October 25, 2023
Accepted: October 30, 2023
Published: November 17, 2023

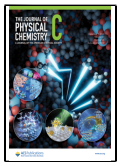

femtosecond timescales, water molecules exhibit microscopic dynamics which include hydrogen bond strengthening, librational motions, and mixed stretch−bend motions.[18,19,21] At the interfaces, hydrogen-bonded (HB) systems are highly dynamic. For instance, one molecule of a water dimer rotates around a second one, as calculated on Pd(111)[22] and experimentally revealed on Pt(111).[23] The water dimer was imaged here as a six-fold flower-like protrusion, reflecting the six symmetry-equivalent positions of the rotating molecule around the static one. This interpretation was put forward for water dimers on Cu(111)[24] and water solvating a Na ion on Cu(100).[25] Both are imaged as round protrusions, despite their elongated geometry.

We analyzed the interactions governing the structure of the $D_2O/Cs^+/Cu(111)$ interface; see ref 26. At mass equivalent coverages above two D_2O molecules per Cs^+ ion, the energy of the modified charge-transfer resonance becomes independent of the Cs coverage. We concluded that on the Cu(111) surface, the Cs−water interaction competes with hydrogen bonding between two water molecules and that the latter is dominant. Due to the large Cs^+ ion, this competition leads to a peculiar structure in which the Cs^+ is located at the perimeter of Cs−water clusters. The work function increased by almost 1 eV upon adsorption of D_2O on $Cs^+/Cu(111)$. We also observe an energy stabilization through a split-off electronic state, contrary to the case of Xe as a nonpolar solvent.[27] Although we have been investigating the variation of hydration dynamics for different alkali ions,[28] a dynamic effect of H-bonding on the electron-transfer dynamics remained elusive.

Here, we investigate the electron-transfer dynamics of alkali ion Cs^+ adsorbed on a Cu(111) electrode in the presence of water as a coadsorbate using femtosecond time-resolved two-photon photoelectron spectroscopy (2PPE) combined with low-temperature scanning tunneling microscopy (STM). We analyze the variation of excited state lifetime and energy stabilization due to energy transfer to the solvent upon variation of the number of water molecules per ion ρ. We identify in both observables different regimes without and with H-bonding being present. A sharp transition between the regimes is assigned to the change from singly to triply solvated Cs^+ ions.

2. EXPERIMENTAL DETAILS

For the experimental setup, the Cu(111) single-crystal serves as a surface and an electrode for electron transfer. It is kept in ultrahigh vacuum (UHV) at a base pressure 2×10^{-10} mbar (5×10^{-10} mbar) for 2PPE (STM) experiments. It is prepared by ion sputtering cycles using Ar at 2×10^{-5} mbar (3×10^{-5} mbar) pressure at 1.5 keV (1.3 keV) ion energy for 10−30 min and subsequent annealing at a temperature $T = 600$ K (893 ± 1 K) for 10−20 min. The investigated Cs^+ ions are chemisorbed on Cu(111) at $T = 200$ K (249 ± 4 K). They are generated as neutral atoms from commercial tertiary sources (SAES getters). The Cs coverage in monolayers (ML) Θ_{Cs} is defined with respect to a closed-packed (2×2) layer on Cu(111). Θ_{Cs} is determined in the 2PPE experiments by measuring the change in work function $\Phi = E_{vac} - E_F$ of the surface upon Cs adsorption, as described in ref 29; E_{vac} and E_F are the vacuum energy and the Fermi energy of Cu(111), respectively. The energy reference of the experiment is E_F since the sample and the spectrometer have a common potential. Liquid water (D_2O) is stored in a test tube as part of the gas system. It is connected to a main and a dosing reservoir. After purification of the water in the test tube through several freeze−pump−thaw cycles, water is introduced at a pressure of 0.1 mbar into the main reservoir. Subsequently, it is expanded into the dosing reservoir and through a pinhole of 50 μm diameter into the UHV for a controlled dosing time at a constant pressure, which are both proportional to the desired water coverage on the Cu(111) surface. The Cu(111) surface is kept in UHV at a temperature of 80 K in front of a stainless-steel tube which guides the water vapor in UHV from the pinhole to the sample. We use heavy water D_2O for technical reasons to distinguish the H_2O background pressure in the UHV chamber from the prepared surface adsorption with D_2O. The D_2O coverage Θ_{D_2O} is quantified by temperature-programmed desorption and measurement of the change in Φ.[30] The amount of dosed water was calibrated previously by water adsorption on Ru(001) in terms of bilayers (BLs).[30] One BL refers to a hexagonal layer with two molecules per three surface atoms, in which neighboring molecules are displaced by 96 pm vertically. Thus, 1 BL refers to a closed single molecular layer of water ice. The determination of Φ by two-photon photoemission spectroscopy (2PPE) allows the determination of mass equivalent coverages as fractions of 1 BL.[30] With this analysis, we obtain the number of respective ions and molecules per surface area, which gives the spatially averaged ratio ρ of D_2O molecules to Cs^+ ions on the Cu(111) surfaces. We varied the coverage ratio ρ from 1 to 7 in our experiments, which corresponds to Cs-water clusters of a few nanometer sizes on Cu(111). The thermal stability of the Cs−water clusters was analyzed by thermal desorption spectroscopy on the Cu(111) surface.[28] In the presence of alkali ions Na, K, and Cs, we observed water desorption at 50, 40, and 15 K higher temperatures, respectively, than that from bare Cu(111) at 160 K. This finding indicates that the investigated alkali−water clusters are stable to temperatures far above 80 K used in the present study.

To analyze the interaction of D_2O with $Cs^+/Cu(111)$, we monitor the dynamic response of the interface upon resonance, photoinduced electron transfer to the Cs 6s-derived wave function with an increasing number of water molecules coadsorbed onto the surface in femtosecond time-resolved 2PPE, as illustrated in Figure 1.

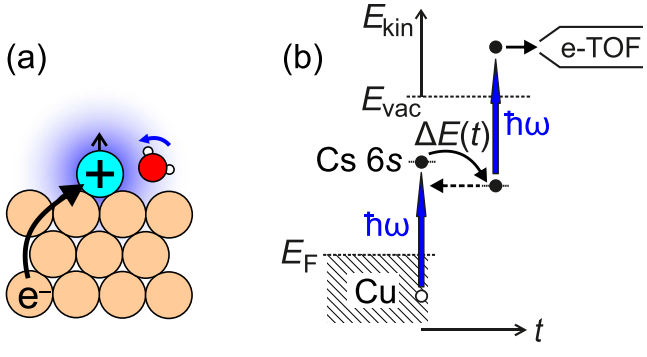

Figure 1. (a) Illustration of this photoexcited electron transfer in real space from the Cu bulk to the adsorbed ion and potential response of the surrounding water to the modified ion charge. (b) Scheme of photoexcited electron transfer from the Cu surface to the Cs 6s orbital of the alkali ion adsorbed on the Cu(111) surface and time-resolved two-photon photoelectron spectroscopy. The kinetic energy of photoelectron E_{kin} is analyzed by an electron time-of-flight spectrometer (e-TOF).

https://doi.org/10.1021/acs.jpcc.3c06172
J. Phys. Chem. C 2023, 127, 23467−23474

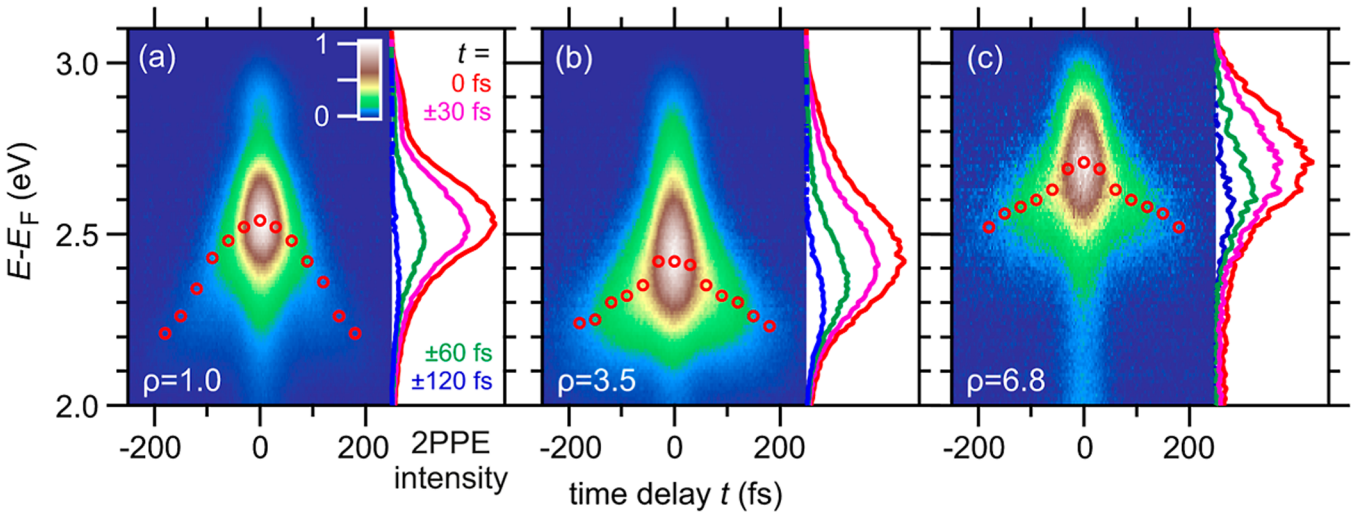

Figure 2. (a–c) Measured data sets of time-resolved 2PPE intensity autocorrelations with increasing coverage ratio ρ (number of water molecules per adsorbed ion) after subtraction of a time-independent background signal. In each individual panel, the intensity is shown in a false color representation as a function of time delay and intermediate state energy $E - E_F$ at the left and as spectra at selected time delays after averaging negative and positive time delays at right. The open red circles indicate the energy of the intensity maxima at the respective time delay. The data were recorded at a temperature of 80 K.

In the 2PPE experiment, two photons of energy $\hbar\omega$ = 3.1 eV, which is below the work function Φ, are absorbed and emit one photoelectron with kinetic energy E_{kin}. As illustrated in Figure 1b, one photon from a first femtosecond laser pulse excites resonant electron transfer from Cu(111) to the unoccupied Cs 6s state of the adsorbed Cs^+ ion.[31−34] A second photon from a second laser pulse at a time delay of t generates the photoelectrons analyzed in an electron time-of-flight spectrometer. Femtosecond laser pulses at a 1.55 eV photon energy and 40 fs pulse duration are generated in a commercial Ti/sapphire amplifier (Coherent RegA 9040) and frequency doubled in BaB_2O_4 to $\hbar\omega$ = 3.10 eV. For details of the experimental setup, see ref 35. From the measured E_{kin}, we calculate the energy with respect to the energy reference E_F

$$E - E_F = E_{kin} + \Phi - 2\hbar\omega \quad (1)$$

with the work function Φ, which is determined from the highest kinetic energy in the 2PPE spectrum by $E_{kin}^{max} = 2\hbar\omega - \Phi$.

Density functional theory (DFT) calculations using PBE[36] with D3 dispersion corrections[37,38] were performed using VASP.[39,40] The Cu(111) surface is modeled by a three-layer 5 × 5 unit cell. Additional details on the DFT calculations, as well as the cluster structures, are presented in the Supporting Information of ref 26. For the present work, numerical vibrational frequency calculations using central differences with a displacement of 1.5 pm were performed.

For the STM experiment, the water is purified in a glass tube by several freeze–pump–thaw cycles before it was introduced into a dedicated molecule deposition chamber via a leak valve. At a vapor pressure of approximately 5 × 10^{-5} mbar, it is expanded into the preparation and STM chamber, reducing the pressure by several orders of magnitude. The water is deposited onto the sample situated within the cold shields surrounding the STM for approximately 1.5 s. During deposition, the sample temperature rises slightly to less than 13 K. The D_2O coverage of 0.34% BL is determined from pure water structures on the pristine metal resulting from the same procedure.

3. RESULTS AND DISCUSSION

Figure 2 shows time-resolved 2PPE intensity autocorrelation measurements for ρ = 1.0, 3.5, and 6.8. In such an autocorrelation measurement, two identical laser pulses are used in a pump–probe configuration, and the change as a function of nominally positive and negative time delays are identical. Therefore, the observed changes are monotonic as a function of the time delay. The pronounced peak at t = 0 represents the photoinduced electron-transfer resonance from electronic states in Cu near E_F to the 6s-derived state of Cs^+/Cu(111).[34] Two effects are recognized immediately. First, the energy of the electron-transfer resonance shifts nonmonotonously with ρ. This behavior results from the variation of the static electronic and geometric structure with ρ, see Ref. 26 Second, the time-dependent dynamics depends on ρ. For smaller ρ, the intensity decays faster, and the overall peak energy shift is higher compared to larger ρ, see the red circles in Figure 2. These effects represent water-induced variations in the interaction of the Cs 6s-derived wave function with the electronic states in Cu(111) and energy transfer in response to nuclear motion, respectively.

For further analysis of the transient electron population, the time-dependent 2PPE intensity was integrated within an energy interval of 1 eV to include the entire electron transfer peak in the 2PPE spectrum. The intensity is normalized at t = 0 for different ρ. The results are depicted in Figure 3a. The obtained time-dependent population traces exhibit two regimes (ρ > 2 and ρ < 2) with identical behavior within each regime. While in both the regimes, the decay is clearly slower than that for bare Cs^+/Cu(111) at ρ = 0,[31−34] the decay time increases with ρ. We fit these experimental data with a single-exponential relaxation convoluted with a Gaussian which represents the laser pulse autocorrelation; see the solid lines in Figure 3a. This fit describes the single-exponential relaxation observed for |t| > 30 fs very well. For |t| < 30 fs, the fit deviates from the experimental data, which is explained by coherent 2PPE processes that do not lead to electron transfer to the Cs 6s state. A population build-up requires phase-breaking events

https://doi.org/10.1021/acs.jpcc.3c06172
J. Phys. Chem. C 2023, 127, 23467−23474

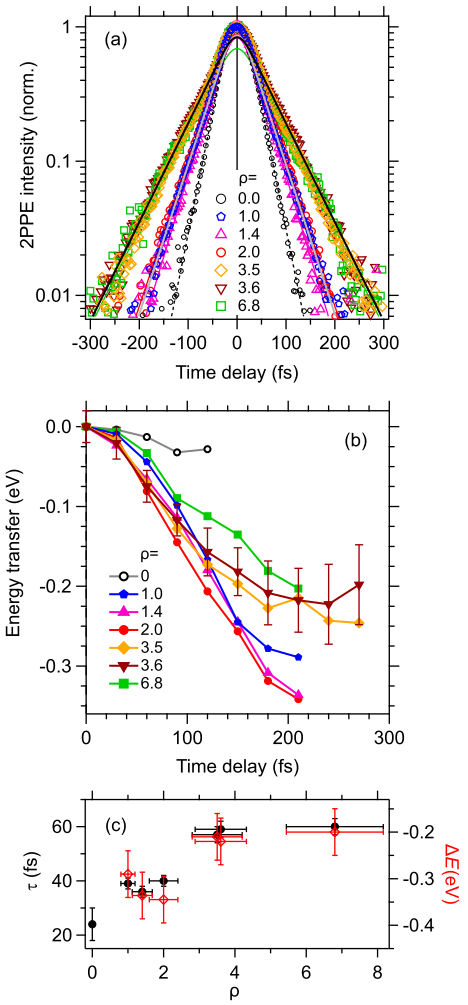

Figure 3. (a) Energy-integrated time-dependent intensity of the 2PPE autocorrelation for different coverage ratio ρ is indicated by different symbols. $\rho = 0$ is a reference measurement for bare $Cs^+/Cu(111)$ without coadsorbed water. Lines are the results of modeling the single-exponential decay with relaxation time τ convoluted with a Gaussian to describe the autocorrelation of the UV laser pulses. The gray line describes the data for $\rho = 1.0$, and the black line $\rho = 3.5$. The color of the further lines indicates ρ according to the legend. (b) Time-dependent energy transfer from the electronic to the nuclear degree of freedom determined from the energy shift of Cs 6s resonance in the time-resolved 2PPE spectra for different coverage ratios ρ. Data for negative and positive t are averaged. The vertical error bars indicated for $\rho = 3.6$ are representative of all ρ. (c) Filled black circles represent the relaxation times (left axis) as a function of ρ determined by the single-exponential decay fit to the data in (a). The value at $\rho = 0$ is a reference value representing the chosen data analysis by exponential decay times.[31−34] Open symbols in red depict the energy transfer (right axis) of the Cs 6s resonance to nuclear motion taken from the data shown in (b) at a time delay of 210 fs.

which lead to an incoherent 2PPE contribution,[41,42] which follows the exponential decay with a decay time τ.

Figure 3c represents the obtained values for τ as a function of ρ. The fit results for τ upon adsorption of D_2O indicate an increase in τ to ∼40 fs for $\rho < 2$ and to ∼60 fs for $\rho > 2$ in two distinctive steps. As discussed by Gauyacq et al.,[34] the decay time measured in time-resolved 2PPE intensity is due to elastic wavepacket propagation from the localized Cs 6s wave function to delocalized Bloch states in Cu(111). An increase in lifetime upon water coadsorption to $Cs^+/Cu(111)$, as observed in Figure 3a, implies that already few water molecules weaken the electronic Cs−Cu interaction considerably since they are polarized upon electron transfer to Cs^+ which results in screening of the interaction. While in dielectric environments, like Xe,[27,43] screening can be strong due to the large electron density ($Z = 54$), in water with 18 electrons, the molecular dipole will lead to considerable screening by its reorientation in the hydration response. Note that on the same $Cs^+/Cu(111)$ surface, we observed a six-time increase in τ for Xe coadsorption compared to a 2.5 times increase in the case of D_2O. We attribute the increase of τ in the case of water coadsorption to dipolar screening rather than to dielectric screening. The occurrence of two distinct structural regimes above and below $\rho = 2$ indicates that besides the dipolar character, the static structure plays an important role. Considering the frequency-dependent dielectric constant of water ice,[44] it is plausible that the strength of dynamic, dipolar screening effects indeed depends on the orientation of the molecular dipole and its response to a change of the charge count of the alkali ion as in these experiments induced by resonant charge transfer on the femtosecond time scale.

With the time-dependent energy shift ΔE of the electron-transfer state, we analyze the hydration dynamics, which is possible since Φ is constant as a function of t within the energy resolution of 50 meV as measured at the low energy cutoff of the 2PPE spectrum. The sign of ΔE is assumed to be negative upon the transfer of energy from the electronic system to the solvent. We determine the time-dependent shift of the peak maxima of the 2PPE spectra, see Figure 2, for different ρ. The results are reported in Figure 3b. The two structural regimes below and above $\rho = 2$ which were mentioned above also affect this dynamic observable. For $0 < \rho \leq 2$, the energy $\Delta E = 0.3$ eV is transferred to hydration modes within 210 fs. For $2 < \rho < 7$, the energy transfer is 0.2 eV within the same time window. Figure 3c further depicts the amount of total energy stabilization of the peak energy as a function of ρ. It also depicts two different regimes below and above $\rho = 2$ which resembles the lifetime dependence on ρ. The longer lifetimes $\rho > 2$ allow us to analyze the energy gain up to larger time delays than that for $\rho < 2$.

We explain the two distinct regimes in the electron lifetime and the energy stabilization by a different solvent response of water on the transiently recharged Cs upon electron transfer in the absence and presence of H-bonding below and above $\rho = 2$, respectively. In our earlier work, we analyzed the geometric and the electronic structure.[26] We concluded a peculiar inside-out solvation structure for the higher water coverage and appearance of a second electronic state lower in energy at $\rho = 2$ which are explained by competing interactions at the interface dominated by H-bonding.

In order to validate the onset of H-bonding on $\rho = 2$ further, we calculated the harmonic vibrational frequencies of the water molecules in the solvated species $Cs^+−H_2O$ on Cu(111) using DFT. This is additional information, independent of the experimental results, and characterizes the water−water interaction. Focusing on the modes above 1000 cm^{-1}, there are two main types of vibrations: O−H stretch vibrations (above 3000 cm^{-1}) and H−O−H bending vibrations (around 1600 cm^{-1}). The O−H bonds and the corresponding stretching vibrations can be further divided into HB and free or non-HB, OH groups. The non-HB frequencies are higher than the HB ones (see Figure 4), and they are mostly independent of the water coverage. In contrast, HB frequencies

https://doi.org/10.1021/acs.jpcc.3c06172
J. Phys. Chem. C 2023, 127, 23467−23474

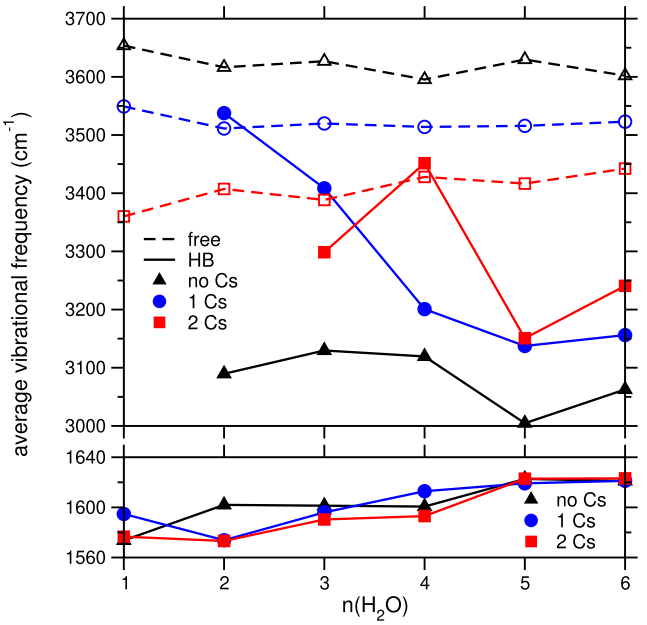

Figure 4. Harmonic vibrational frequencies of the water molecules in Cs^+−H_2O clusters on Cu(111), averaged over all of the respective modes, as a function of water coverage. The upper panel shows the O−H stretch vibrations, divided into hydrogen-bonded (HB, filled symbols) and free (open symbols) OH groups. The lower panel depicts bending modes.

decrease with an increase in water coverage by more than 10%. While the free OH modes are systematically red-shifted with increasing Cs coverage, the HB stretch frequencies are mostly blue-shifted. Bending modes are slightly blue-shifted with increasing water coverage but are independent of the Cs coverage. These frequency shifts due to increasing water coverage agree very well with previous experimental and theoretical work upon the onset of hydrogen bonding.[13,45] Note that these trends are not strongly affected by the presence of Cs, even if the stretch frequencies themselves depend on Cs coverage. We did not aim to accurately reproduce experimental vibrational frequencies with these calculations. Instead, they are meant to show how the water and Cs coverages qualitatively affect water vibrations. There are several factors affecting the accuracy of the calculated frequencies, such as the use of an approximate density functional, the neglect of anharmonic effects, and the use of H_2O instead of D_2O, which are discussed in the literature.[45−47]

A naive expectation of the energy transfer to the solvent could be that the more water molecules that participate in the solvation process, the more energy can be transferred. However, our results show that the contrary is correct. As depicted in Figure 3b, the energy transfer measured for $\rho \leq 2$ is 50% larger than that for more than two water molecules per ion. Considering that at $\rho = 2$, hydrogen bonding sets in—which is not surprising since at least two water molecules are required to form a hydrogen bond between two water molecules—the reduced energy transfer to the solvent for $\rho > 2$ is explained by a competing interaction. Hydrogen bonding leads to the formation of a water network, which results in a reduced mobility compared to individual decoupled water molecules and explains our observation. The competition between energy transfer to the solvent and hydrogen bonding becomes very clear if the energy transfer ΔE, which is decreasing as a function of ρ from 0.3 to 0.2 eV, is compared to typical values of hydrogen bonding of 0.21 eV for the water dimer.[14] Finally, both energies are very similar and may compete. The effect of water on the electronic lifetime as a function of ρ for hydrated Cs^+ ions on Cu(111) is the opposite in this context. For a higher number of water molecules within the cluster, the water network is less mobile due to the water−water interaction (or H-bonding) and might screen the ion−metal interaction better compared to a smaller number of water molecules, which is highly mobile. More water hence supports the localization of the electron to the ion and increases the lifetime.

To support our claim and elucidate the sharp transition, we performed low-temperature STM measurements of Cs^+−D_2O clusters formed on Cu(111) at 13 K under a vast Cs excess. Imaging at very small voltages yields two species that differ in size and symmetry. The main species (89%) is torus-like with a fine structure of three-fold symmetry (Figure 5a). The distance between the maxima on the torus is 0.44 nm. The second most common species (11%) has flower-like six-fold symmetry (Figure 5b). The maxima of both species are aligned along the ⟨112⟩ surface directions.

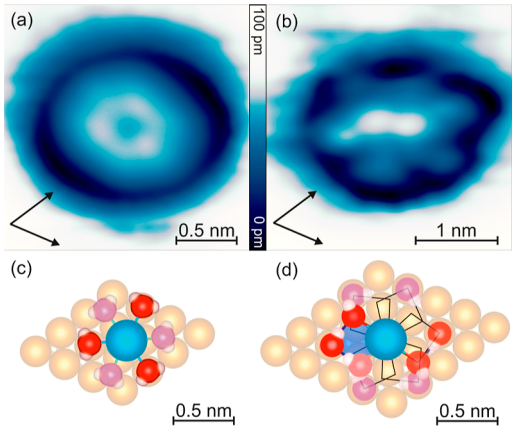

Figure 5. D_2O−Cs^+ solvatomers on Cu(111): (a,b) STM images of singly solvated Cs^+ of three-fold symmetry (a) and triply solvated Cs^+ of six-fold symmetry (b) on different scales as marked; arrows mark two of the ⟨110⟩ surface directions. (c,d) Scheme of six rotamers of singly solvated Cs^+ (c) and triply solvated Cs^+ (d) around the Cs^+ at hollow (c) and on-top site (d). Optimized adsorption structure from,[26] SI; red and magenta oxygen atoms mark D_2O molecules yielding larger and smaller apparent heights in the STM images, respectively. For clarity, the three water molecules are displayed only for one of the rotamers in (d), two in solid red, and one in half-transparent red framing a blue-shaded rhombus, and the others are sketched by rhombi with only the outer water molecule displayed. The STM images were recorded at (a) I = 64 pA and V = 12 mV and (b) I = 150 pA and V = 9 mV.

Lateral size and a large excess of Cs suggest that the smaller species is a singly solvated Cs^+, imaged at six centrosymmetric positions around an anchoring center, the Cs^+. Such a time-averaged STM image of six rotamers resembles that of water dimers on Pt(111),[23] explaining also the round shape of water dimers on Pd(111)[22] and Cu(111).[24] The three-fold symmetry is consistent with the Cs^+ adsorbed in a hollow site, such that for three rotamers, the water molecules are imaged higher in their on-top positions than that in the hollow sites of the other three rotamers.

https://doi.org/10.1021/acs.jpcc.3c06172
J. Phys. Chem. C 2023, 127, 23467−23474

The considerably larger size of the second most common species suggests the presence of a second solvation shell. The second shell exists for the triply but not the doubly solvated Cs^+ according to the optimized adsorption structure,[26] SI. It is coordinated via two hydrogen bonds to the two inner water molecules (Figure 5d, blue shaded rhombus). The six rotamers of triply solvated Cs^+ largely resemble the imaged structure. Thereby, the two higher-imaged protrusions in the interior of the flower-like structure are situated above the water molecules with a hydrogen atom pointing away from the surface. Such water molecules are known to be imaged at a larger apparent height than those with the hydrogen bonds in parallel to the surface.[48,49] The larger apparent height along the main scanning directions is related to the tip−solvatomer interaction that is necessary to image a substructure within the rotamers.

The STM images suggest a system composed of singly and triply solvated Cs^+ without doubly solvated Cs^+. It is supported by calculations published earlier,[26] SI. A singly together with a triply solvated Cs^+ is 30 meV lower in energy than two doubly solvated Cs^+. Hence, the sharp transition between the lifetimes (Figure 3c) is related to the absence of doubly solvated Cs^+. Furthermore, the transition from singly solvated to triply solvated is accompanied by the beginning of a formation of a water network because of the hydrogen bonding within the solvation shell of the triply solvated Cs^+-solvatomers. From the electron-transfer dynamics of the hydrated Cs^+ ions on Cu(111), we can conclude that the ion−solvent interaction at the interface is microscopically determined by a competition between Cs^+−water and water−water interactions. For more than two water molecules per ion, the hydrogen bond between the water molecules is dominant and reduces the energy transfer to the solvent by 50% compared with a single water molecule. Since we observe a weaker energy transfer and longer lifetime for larger ρ, we conclude that the local water network in these hydrated Cs^+ clusters on Cu(111) hinders dipolar rearrangement due to an increased water−water coordination compared to small ρ where less water molecules without formation of a network are present. In this study, the combination of nanoscale structural analysis and a correlation of the energy stabilization with the vibrational frequencies of the water molecules on the Cs^+/Cu(111) interface facilitates the identification of H-bonding as a dominant factor in electron-transfer dynamics.

4. CONCLUSIONS

We conclude that the number of water molecules solvating an ion on a metal surface is decisive for understanding the electron-transfer dynamics across such interfaces. We find that a single water molecule attached to Cs^+ is more mobile and exhibits a stronger response in terms of charge screening and energy gain upon electron transfer. Such a configuration exhibits a 30% faster response compared to that of a hydrogen-bonded arrangement of three water molecules surrounding the ion. For the same reason, the energy gain upon solvation is larger for a single water molecule. The pronounced water coverage dependence of the dynamic observables with a characteristic fingerprint at the onset of hydrogen bonding between water molecules guided the conclusion of the importance of molecular solvent rearrangement rather than that of charge transfer to hydrogen as an electron acceptor. We furthermore found that two water molecules per ion do not occur on the investigated surface. Potentially, a suitable choice of solvent mixtures in which a low-concentration component is attached to the ion to generate energy transfer to the solvent, while the major fraction acts as a screening dielectric, will facilitate the control of electron-transfer rates across interfaces.

AUTHOR INFORMATION

Corresponding Author

Uwe Bovensiepen − *Faculty of Physics and Center for Nanointegration (CENIDE, University of Duisburg-Essen, Duisburg 47057, Germany; Institute for Solid State Physics, The University of Tokyo, Chiba 277-8581 Kashiwa, Japan;* orcid.org/0000-0002-1506-4491; Email: uwe.bovensiepen@uni-due.de

Authors

John Thomas − *Faculty of Physics and Center for Nanointegration (CENIDE, University of Duisburg-Essen, Duisburg 47057, Germany;* Present Address: Max-Born-Institute, 12489 Berlin, Germany

Jayita Patwari − *Faculty of Physics and Center for Nanointegration (CENIDE, University of Duisburg-Essen, Duisburg 47057, Germany; Physical Chemistry I, Ruhr-University Bochum, Bochum 44801, Germany;* orcid.org/0000-0001-5085-8820

Inga Christina Langguth − *Physical Chemistry I, Ruhr-University Bochum, Bochum 44801, Germany*

Christopher Penschke − *Department of Chemistry, University of Potsdam, Potsdam-Golm D-14476, Germany;* orcid.org/0000-0002-0117-7479

Ping Zhou − *Faculty of Physics and Center for Nanointegration (CENIDE, University of Duisburg-Essen, Duisburg 47057, Germany*

Karina Morgenstern − *Physical Chemistry I, Ruhr-University Bochum, Bochum 44801, Germany*

Complete contact information is available at: https://pubs.acs.org/10.1021/acs.jpcc.3c06172

Notes

The authors declare no competing financial interest.

ACKNOWLEDGMENTS

Funding by the Deutsche Forschungsgemeinschaft (DFG, German Research Foundation) under Germany's Excellence Strategy—EXC 2033-390677874-RESOLV, EXC 2008/1-390540038-UniSysCat, and by Project-ID 278162697-SFB 1242 is greatly acknowledged. Furthermore, we acknowledge funding by the European Union through the Horizon 2020 research and innovation program under the Marie Sklodowska-Curie Grant agreement no. 801459-FP-RESOMUS. We would like to thank P. Saalfrank for fruitful discussion.

REFERENCES

(1) O'Regan, B.; Grätzel, M. A low-cost, high-efficiency solar cell based on dye-sensitized colloidal TiO_2 films. *Nature* **1991**, *353*, 737−740.

(2) Fujishima, A.; Honda, K. Electrochemical photolysis of water at a semiconductor electrode. *Nature* **1972**, *238*, 37−38.

(3) Roy, S.; Bryantsev, V. S. Finding order in the disordered hydration shell of rapidly exchanging water molecules around the heaviest alkali Cs^+ and Fr^+. *J. Phys. Chem. B* **2018**, *122*, 12067−12076.

(4) Lee, Y.; Thirumalai, D.; Hyeon, C. Ultrasensitivity of water exchange kinetics to the size of metal ion. *J. Am. Chem. Soc.* **2017**, *139*, 12334−12337.

(5) Bragg, A. E.; Glover, W. J.; Schwartz, B. J. Watching the solvation of atoms in liquids one solvent molecule at a time. *Phys. Rev. Lett.* **2010**, *104*, 233005.
(6) Swanson, J. M. J.; Maupin, C. M.; Chen, H.; Petersen, M. K.; Xu, J.; Wu, Y.; Voth, G. A. Proton Solvation and Transport in Aqueous and Biomolecular Systems: Insights from Computer Simulations. *J. Phys. Chem. B* **2007**, *111*, 4300−4314.
(7) Kratochvil, H. T.; Carr, J. K.; Matulef, K.; Annen, A. W.; Li, H.; Maj, M.; Ostmeyer, J.; Serrano, A. L.; Raghuraman, H.; Moran, S. D.; et al. Instantaneous ion configurations in the K^+ ion channel selectivity filter revealed by 2D IR spectroscopy. *Science* **2016**, *353*, 1040−1044.
(8) Cao, Z.; Peng, Y.; Yan, T.; Li, S.; Li, A.; Voth, G. A. Mechanism of fast proton transport along one-dimensional water chains confined in carbon nanotubes. *J. Am. Chem. Soc.* **2010**, *132*, 11395−11397.
(9) Pean, C.; Daffos, B.; Rotenberg, B.; Levitz, P.; Haefele, M.; Taberna, P.-L.; Simon, P.; Salanne, M. Confinement, desolvation, and electrosorption effects on the diffusion of ions in nanoporous carbon electrodes. *J. Am. Chem. Soc.* **2015**, *137*, 12627−12632.
(10) Ong, M. T.; Verners, O.; Draeger, E. W.; van Duin, A. C. T.; Lordi, V.; Pask, J. E. Lithium ion solvation and diffusion in bulk organic electrolytes from first-principles and classical reactive molecular dynamics. *J. Phys. Chem. B* **2015**, *119*, 1535−1545.
(11) Ball, P. Water as an active constituent in cell biology. *Chem. Rev.* **2008**, *108*, 74−108.
(12) Pérez Paz, A.; Rubio, A. Hydrated alkali atoms on copper(111): a density functional theory study. *J. Phys. Chem. C* **2021**, *125*, 3868−3879.
(13) Nibbering, E. T. J.; Dreyer, J.; Kühn, O.; Bredenbeck, J.; Hamm, P. J.; Elsaesser, T. Vibrational dynamics of hydrogen bonds. In *Analysis and control of ultrafast photoinduced reactions*; Kühn, O., Wöste, L., Eds.; Springer: Berlin, 2007; pp 619−687.
(14) Xantheas, S. S.; Dunning, T. H. J. Ab initio studies of cyclic water clusters $(H_2O)_n$, n = 1−6. I. Optimal structures and vibrational spectra. *J. Chem. Phys.* **1993**, *99*, 8774−8792.
(15) de Rege, P. J. F.; Williams, S. A.; Therien, M. J. Direct evaluation of electronic coupling mediated by hydrogen bonds: implications for biological electron transfer. *Science* **1995**, *269*, 1409−1413.
(16) Berg, N.; Bergwinkl, S.; Nuernberger, P.; Horinek, D.; Gschwind, R. M. Extended Hydrogen Bond Networks for Effective Proton-Coupled Electron Transfer (PCET) Reactions: The Unexpected Role of Thiophenol and Its Acidic Channel in Photocatalytic Hydroamidations. *J. Am. Chem. Soc.* **2021**, *143*, 724−735.
(17) Chen, W.; Guo, S.; Qin, L.; Li, L.; Cao, X.; Zhou, J.; Luo, Z.; Fang, G.; Liang, S. Hydrogen bond-functionalized massive solvation modules stabilizing bilateral interfaces. *Adv. Funct. Mater.* **2022**, *32*, 2112609.
(18) Cowan, M. L.; Bruner, B. D.; Huse, N.; Dwyer, J. R.; Chugh, B.; Nibbering, E. T. J.; Elsaesser, T.; Miller, R. J. D. Ultrafast memory loss and energy redistribution in the hydrogen bond network of liquid H_2O. *Nature* **2005**, *434*, 199−202.
(19) Yang, J.; Dettori, R.; Nunes, J. P. F.; List, N. H.; Biasin, E.; Centurion, M.; Chen, Z.; Cordones, A. A.; Deponte, D. P.; Heinz, T. F.; et al. Direct observation of ultrafast hydrogen bond strengthening in liquid water. *Nature* **2021**, *596*, 531−535.
(20) Nome, R. A. Ultrafast dynamics of solvation: the story so far. *J. Braz. Chem. Soc.* **2010**, *21*, 2189−2204.
(21) Ramasesha, K.; De Marco, L.; Mandal, A.; Tokmakoff, A. Water vibrations have strongly mixed intra and intermolecular character. *Nature* **2013**, *5*, 935−940.
(22) Ranea, V. A.; Michaelides, A.; Ramírez, R.; de Andres, P. L.; Vergés, J. A.; King, D. A. Water Dimer Diffusion on Pd{111} Assisted by an H-Bond Donor-Acceptor Tunneling Exchange. *Phys. Rev. Lett.* **2004**, *92*, 136104.
(23) Motobayashi, K.; Matsumoto, C.; Kim, Y.; Kawai, M. Vibrational study of water dimers on Pt(111) using a scanning tunneling microscope. *Surf. Sci.* **2008**, *602*, 3136−3139.
(24) Bertram, C.; Fang, W.; Pedevilla, P.; Michaelides, A.; Morgenstern, K. Anomalously low barrier for water dimer diffusion on Cu(111). *Nano Lett.* **2019**, *19*, 3049−3056.
(25) Shiotari, A.; Okuyama, H.; Hatta, S.; Aruga, T.; Hamada, I. Atomic-scale study of the formation of sodium-water complexes on Cu(110). *Phys. Chem. Chem. Phys.* **2018**, *20*, 12210−12216.
(26) Penschke, C.; Thomas, J.; Bertram, C.; Michaelides, A.; Morgenstern, K.; Saalfrank, P.; Bovensiepen, U. Hydration at highly crowded interfaces. *Phys. Rev. Lett.* **2023**, *130*, 106202.
(27) Thomas, J.; Bertram, C.; Daru, J.; Patwari, J.; Langguth, I.; Zhou, P.; Marx, D.; Morgenstern, K.; Bovensiepen, U. Competition between Coulomb and van der Waals interactions in Xe-Cs^+ aggregates on Cu(111) surfaces. *Phys. Rev. Lett.* **2021**, *127*, 266802.
(28) Meyer, M.; Agarwal, I.; Wolf, M.; Bovensiepen, U. Ultrafast electron dynamics at water covered alkali adatoms adsorbed on Cu(111). *Phys. Chem. Chem. Phys.* **2015**, *17*, 8441−8448.
(29) Lu, Q. B.; O'Connor, D.; King, B. V.; MacDonald, R. J. Local electrostatic potential determination of surfaces by negative ion spectroscopy. *Surf. Sci.* **1996**, *347*, L61−L65.
(30) Bovensiepen, U.; Gahl, C.; Wolf, M. Solvation dynamics and evolution of the spatial extent of photoinjected electrons in D_2O/Cu(111). *J. Phys. Chem. B* **2003**, *107*, 8706−8715.
(31) Bauer, M.; Pawlik, S.; Aeschlimann, M. Resonance lifetime and energy of an excited Cs state on Cu(111). *Phys. Rev. B* **1997**, *55*, 10040−10043.
(32) Ogawa, S.; Nagano, H.; Petek, H. Phase and Energy Relaxation in an Antibonding Surface State: Cs/Cu(111). *Phys. Rev. Lett.* **1999**, *82*, 1931−1934.
(33) Petek, H.; Weida, M. J.; Nagano, H.; Ogawa, S. Real-time observation of adsorbate atom motion above a metal surface. *Science* **2000**, *288*, 1402−1404.
(34) Gauyacq, J. P.; Borisov, A. G.; Bauer, M. Excited states in the alkali/noble metal surface systems: A model system for the study of charge transfer dynamics at surfaces. *Prog. Surf. Sci.* **2007**, *82*, 244−292.
(35) Sandhofer, M.; Sklyadneva, I. Y.; Sharma, V.; Trontl, V. M.; Zhou, P.; Ligges, M.; Heid, R.; Bohnen, K. P.; Chulkov, E. V.; Bovensiepen, U. Unoccupied electronic structure and relaxation dynamics of Pb/Si(111). *J. Electron Spectrosc. Relat. Phenom.* **2014**, *195*, 278−284.
(36) Perdew, J. P.; Burke, K.; Ernzerhof, M. Generalized gradient approximation made simple. *Phys. Rev. Lett.* **1996**, *77*, 3865−3868.
(37) Grimme, S.; Antony, J.; Ehrlich, S.; Krieg, H. A consistent and accurate ab initio parametrization of density functional dispersion correction (DFT-D) for the 94 elements H-Pu. *J. Chem. Phys.* **2010**, *132*, 154104.
(38) Grimme, S.; Ehrlich, S.; Goerigk, L. Effect of the damping function in dispersion corrected density functional theory. *J. Comput. Chem.* **2011**, *32*, 1456−1465.
(39) Kresse, G.; Furthmüller, J. Efficiency of ab-initio total energy calculations for metals and semiconductors using a plane-wave basis set. *Comput. Mater. Sci.* **1996**, *6*, 15−50.
(40) Kresse, G.; Furthmüller, J. Efficient iterative schemes for ab initio total-energy calculations using a plane-wave basis set. *Phys. Rev. B* **1996**, *54*, 11169−11186.
(41) Petek, H.; Ogawa, S. Femtosecond time-resolved two-photon photoemission studies of electron dynamics in metals. *Prog. Surf. Sci.* **1997**, *56*, 239−310.
(42) Weinelt, M. Time-resolved two-photon photoemission from metal surfaces. *J. Phys.: Condens. Matter* **2002**, *14*, R1099−R1141.
(43) Chiang, T.-C.; Kaindl, G.; Mandel, T. Layer-resolved shifts of photoemission and Auger spectra from physisorbed rare-gas multilayers. *Phys. Rev. B* **1986**, *33*, 695−711.
(44) Takei, I.; Maeno, N. Dielectric Low-Frequency Dispersion and Crossover Phenomena of HCl-Doped Ice. *J. Phys. Chem. B* **1997**, *101*, 6234−6236.
(45) Dunn, M. E.; Evans, T. M.; Kirschner, K. N.; Shields, G. C. Prediction of accurate anharmonic experimental vibrational frequen-

https://doi.org/10.1021/acs.jpcc.3c06172
J. Phys. Chem. C 2023, 127, 23467−23474

cies for water clusters, $(H2O)_n$, n = 2−5. *J. Phys. Chem. A* **2006**, *110*, 303−309.
(46) Kesharwani, M. K.; Brauer, B.; Martin, J. M. L. Frequency and zero-point vibrational energy scale factors for double-hybrid density functionals (and other selected methods): can anharmonic force fields be avoided? *J. Phys. Chem. A* **2015**, *119*, 1701−1714.
(47) Ceriotti, M.; Fang, W.; Kusalik, P. G.; McKenzie, R. H.; Michaelides, A.; Morales, M. A.; Markland, T. E. Nuclear quantum effects in water and aqueous systems: experiment, theory, and current challenges. *Chem. Rev.* **2016**, *116*, 7529−7550.
(48) Carrasco, J.; Michaelides, A.; Forster, M.; Haq, S.; Raval, R.; Hodgson, A. A one-dimensional ice structure built from pentagons. *Nat. Mater.* **2009**, *8*, 427−431.
(49) Morgenstern, K.; Nieminen, J. Intermolecular Bond Length of Ice on Ag(111). *Phys. Rev. Lett.* **2002**, *88*, 066102.

https://doi.org/10.1021/acs.jpcc.3c06172
J. Phys. Chem. C 2023, 127, 23467−23474